Biomaterials Science

ROYAL SOCIETY OF CHEMISTRY

PAPER

View Article Online
View Journal | View Issue

Cite this: *Biomater. Sci.*, 2020, **8**, 1711

Microencapsulation improves chondrogenesis *in vitro* and cartilaginous matrix stability *in vivo* compared to bulk encapsulation†

Fanyi Li,‡§[a,b] Clara Levinson,‡[c] Vinh X. Truong,[a] Lee Ann Laurent-Applegate,[d] Katharina Maniura-Weber,[e] Helmut Thissen,[b] John S. Forsythe,[a] Marcy Zenobi-Wong*[c] and Jessica E. Frith*[a]

The encapsulation of cells into microgels is attractive for applications in tissue regeneration. While cells are protected against shear stress during injection, the assembly of microgels after injection into a tissue defect also forms a macroporous scaffold that allows effective nutrient transport throughout the construct. However, in most of current strategies that form microgel-based macroporous scaffold or higher-order structures, cells are seeded during or post the assembly process and not microencapsulated *in situ*. The objective of this study is to investigate the chondrogenic phenotype of microencapsulated fetal chondrocytes in a biocompatible, assembled microgel system *vs*. bulk gels and to test the stability of the constructs *in vivo*. Here, we demonstrate that cell microencapsulation leads to increased expression of cartilage-specific genes in a TGF-β1-dependent manner. This correlates, as shown by histological staining, with the ability of microencapsulated cells to deposit cartilaginous matrix after migrating to the surface of the microgels, while keeping a macroscopic granular morphology. Implantation of precultured scaffolds in a subcutaneous mouse model results in vessel infiltration in bulk gels but not in assembled microgels, suggesting a higher stability of the matrix produced by the cells in the assembled microgel constructs. The cells are able to remodel the microgels as demonstrated by the gradual disappearance of the granular structure *in vivo*. The biocompatible microencapsulation and microgel assembly system presented in this article therefore hold great promise as an injectable system for cartilage repair.

Received 21st September 2019,
Accepted 8th January 2020

DOI: 10.1039/c9bm01524h

rsc.li/biomaterials-science

1. Introduction

Autologous chondrocyte implantation (ACI) is the gold standard for cartilage repair and has led to relatively good clinical outcomes. However, the process is invasive, costly, and the delay before actual tissue regeneration is long as it takes at least 26 weeks for the defect to be completely filled with repair tissue.[1] The current state of the art has advanced from simple injection of human articular chondrocytes (hACs) covered by a periosteal flap, to implantation of the cells within a scaffold material.[1] Among these scaffolds, hydrogels have shown great promise and several reviews describe their use in tissue engineering.[2–5]

However, bulk hydrogels have limitations due to the nanometer-sized pore size, which greatly limit cell migration, proliferation and ECM deposition in the case of cell-laden gels, or host cell infiltration in the case of acellular hydrogels.[6] Macroporous scaffolds have been proposed as an alternative,[7,8] as they allow greater diffusion of nutrients to cells throughout the whole scaffold, and they also provide space for cell migration into the implanted scaffold for *in situ* repair. Cell migration into the defect is an important part of the regeneration process,[9] which may explain the improved regeneration with macroporous scaffolds.[10] Microgels are polymer colloid particles, which can be fabricated using various techniques, such as mould-casting based photolithography,[11] electro-spraying,[12] microfluidics[13] or inverse suspension polymerisation.[14]

[a]*Department of Materials Science and Engineering, Monash Institute of Medical Engineering, Monash University, Wellington Road, Clayton, VIC 3800, Australia. E-mail: Jessica.frith@monash.edu*
[b]*CSIRO Manufacturing, Bayview Avenue, Clayton, VIC 3168, Australia*
[c]*Tissue Engineering + Biofabrication, Department of Health Sciences and Technology, ETH Zürich, Switzerland. E-mail: Marcy.zenobi@hest.ethz.ch*
[d]*Unit of Regenerative Therapy, Lausanne University Hospital of Lausanne, Switzerland*
[e]*Empa, Swiss Federal Laboratories for Materials Science and Technology, Laboratory for Biointerfaces, St. Gallen, Switzerland*
†Electronic supplementary information (ESI) available. See DOI: 10.1039/c9bm01524h
‡These authors contributed equally.
§Present address: Murdoch Children's Research Institute, The Royal Children's Hospital, 50 Flemington Road, Parkville, VIC 3052, Australia.

They represent a novel way to produce injectable, ultimately macroporous systems, as an alternative to the use of porogens or emulsions.[15,16] Microgels have found utility in various biomedical applications such as drug delivery systems[17,18] and more recently tissue engineering.[10,13]

In the case of cartilage repair, microgels have been used for various purposes. For instance, they have been used as a platform to investigate the chondrogenic differentiation capacity of mesenchymal stem cells (MSCs) in 3D compared to 2D culture,[2] or as a supporting material to create "artificial microtissues" implanted after *in vitro* preculture.[19] In addition, microgels have been utilized as chondrogenic growth factor delivery systems.[20,21] We have previously introduced the use of gelatin norbornene (GelNB) – poly(ethylene glycol)dithiol (PEGdiSH) microgels as building blocks to safely inject cells for the treatment of cartilage lesions.[22,23] We demonstrated that this material is biocompatible, cell-friendly and that it promotes an enhanced chondrogenic phenotype of encapsulated human mesenchymal stem cells (hMSCs) as compared to a bulk hydrogel system as well as "gold standard" pellet culture.[22] The positive effect of the microgel structure on the maintenance of chondrogenic marker expression has also been demonstrated *in vivo*, therefore underlining the advantages of a bottom-up rather than a top-down approach for cartilage tissue engineering.[19]

Microgel fabrication must allow facile encapsulation of cells with high viability to ultimately protect cells from shear stress damage during arthroscopic injection. In addition, the assembly method should provide relative stability to the final construct, to cope with the mechanically challenging environment of the joint. Several methods have been developed to assemble microgels and form scaffolds with higher porosity for tissue engineering purposes.[24,25] Griffin and colleagues used an enzyme, transglutaminase factor XIII, to crosslink peptides at the surface of the microgels.[10] White light with eosin Y has also been used to crosslink and stabilise HA microgels, thus reducing the processing time to 1 minute.[26] Later, novel click chemistry was used to assemble PEG-based microgels, for example using SPAAC[14] and thiol–ene photo click reactions.[26] More recently, the thermo-responsive behaviour of gelatin was utilised to physically crosslink gelatin methacryloyl (GelMA) microgels at low temperature (4 °C) and then stabilise the structure *via* UV photopolymerisation.[27] In another study, UV light triggered thiol-ene click chemistry was used to crosslink PEG-norbornene microgels with a PEG-dithiol linker.[28] However, despite elegant chemistries, and demonstrated of biocompatibility in the above strategies, cells were incorporated during the microgel crosslinking process and not encapsulated within the microgels. Therefore, cells are grown on the surface of the assembled microgels. Besides, these approaches offer no protection to cells during the injection process. Moreover, the microgel assembly process in some studies are light-triggered or highly temperature sensitive, which make these approaches difficult for use as an injectable system for clinical applications. We have previously introduced an approach using 4-arm PEG-succinimidyl glutaramide (PEG-NHS) to bind GelNB-PEGdiSH microgels, which are fabricated *via* a customised pipette tip-based microfluidic device (the final PEG-NHS treated assembled-microgels is referred to as "NHSA-microgels").[23] The addition of PEG-NHS allowed crosslinking of the microgels and we demonstrated that it was possible to cast the microgel suspension into an *in vitro* cartilage defect model to produce a stable macroporous construct. Furthermore, the viability of the embedded cells was not affected. This makes this strategy promising for the use as an injectable therapy for cartilage lesions.

An important parameter for the successful development of a microgel-based treatment for cartilage lesions is the choice of the cell type to be embedded. ACI uses the patient's own chondrocytes after isolation and 2D expansion to reach a sufficient number of cells and in recent years, most of the cell-based approaches entering clinical trials have relied on the use of autologous chondrocytes despite the lower cell yield,[29] the slower proliferation rate[30] and the tendency of the cells to de-differentiate during *in vitro* culture.[31] To envision a more scalable translational approach, the field has turned towards other cell sources, such as human mesenchymal stem cells (hMSCs) and chondroprogenitors/chondrocytes from fetal[32] and infant[33] origins. MSCs are widely investigated for their immunosuppressive properties and their capacity to differentiate into chondrocytes. We have reported that hMSCs can differentiate into chondrocytes in our gelatin-PEG microgel system.[23] However, there are limited amounts of MSCs in biopsies, and these cells can undergo hypertrophy, further differentiating into osteoblasts.[34–36] These drawbacks call for alternative cell sources that are already advanced in the differentiation process but can still proliferate while keeping their chondrogenic phenotype. A promising alternative is the use of human fetal chondroprogenitor cells (hCCs) isolated from the fetal epiphysis. These cells can retain their chondrogenic potential up to 20 passages[37] and were shown to successfully deposit cartilaginous ECM in several hydrogels *in vitro* and *in vivo*, namely alginate and hyaluronan, for cartilage engineering purposes.[32,38] Due to the high proliferative potential of hCCs, sufficient cells can be generated from one donor (35 billion cells estimated) to treat hundreds of patients, which could reduce the variable clinical results among patients treated with ACI. Indeed, the chondrogenic potential of autologous chondrocytes can vary drastically among patients.[39] More importantly, hCCs have a strong migratory behaviour, which is an important part of the healing process when using microgels,[10] since the cells first migrate to, and proliferate on the surface of the microgels before producing ECM.[23] Therefore, both human articular chondrocytes (hACs) and hCCs were assessed for their suitability as a cell source in the assembled microgel system, with hMSCs serving as the control. In addition, we found most of *in situ* microencapsulated MSCs migrated to the surface of microgels after one week culture and that this facilitated more cell–cell interactions and produced more cartilaginous matrix compared to bulk hydrogels. We hypothesised that the promising chondrogenic differentiation results and cartilaginous matrix production relied upon this distinction

between tissue formation between microgels and within the hydrogel matrix of bulk hydrogels. The initial selection of the cell source was determined based on the criteria of (1) high cell viability following the microfluidic microencapsulation process and (2) fast migration speed of cells from the inner core of the microgels to their surface.

Finally, a limitation of highly porous scaffolds for tissue engineering is their lower structural stability. Before proceeding to further development of a given system, it is important to consider the stability of the microgels and of the ECM deposited by the cells in this system. In this regard, subcutaneous implantation in mice represents a first step towards the understanding of such constructs in a more challenging environment than *in vitro* culture.

The aim of this study is to investigate the cells from different sources with the GelNB-PEGdiSH microgels system. We hypothesize that using the microfluidic technique to microencapsulate cells in microgels and to assemble these cell-laden microgels into a macroporous structure will lead to better chondrogenesis than in conventional bulk gels *in vitro*, and to greater stability *in vivo*.

2. Results and discussion

2.1. Human cell type screening

In order to assess whether the alternative human cell types survive during the microgel fabrication process and are compatible with the gelatin-PEG material, hACs and hCCs, as well as hMSCs (the cell type used in our previous studies) as a control, were *in situ* encapsulated in the 600 μm-diameter microgels with high monodispersity as our previous report[22] (Fig. 1A). Live/dead staining at 24 hours post-encapsulation showed a high viability of over 80% for all three cell types (Fig. 1B and C), with no differences between the different cell sources. This demonstrates that both the *in situ* pipette tip-based microfluidic encapsulation process and the visible light-induced thiol–ene photo click polymerisation are compatible with all three cell types. Further live/dead staining was conducted to monitor cell viability in microgels cultured in basal medium for up to one week (Fig. 1B and C). This showed a significant increase in the proportion of live hACs from day 4 to day 7 (P = 0.0119), which we attribute to the high proliferation rate of hACs in the microgels. After 7 days in culture, this increase in viable hACs resulted in a slightly but significantly higher hAC viability (91 ± 2%) as compared to hMSCs (87 ± 2%, P = 0.0023). hCC viability (89 ± 1%) was not statistically different from that of hMSCs. This is consistent with our previous research showing that gelatin-PEG microgels provide a suitable microenvironment for long-term cell maintenance.[22] The excellent cytocompatibility may be attributed to the gelatin, which is a major component of the microgels and has an intrinsic property for cell adhesion. This is particularly favourable for anchorage-dependent cells, such as the hACs, hCCs and hMSCs that are investigated here. Furthermore, the small dimensions and spherical geometry of the microgels may facilitate rapid nutrient and waste

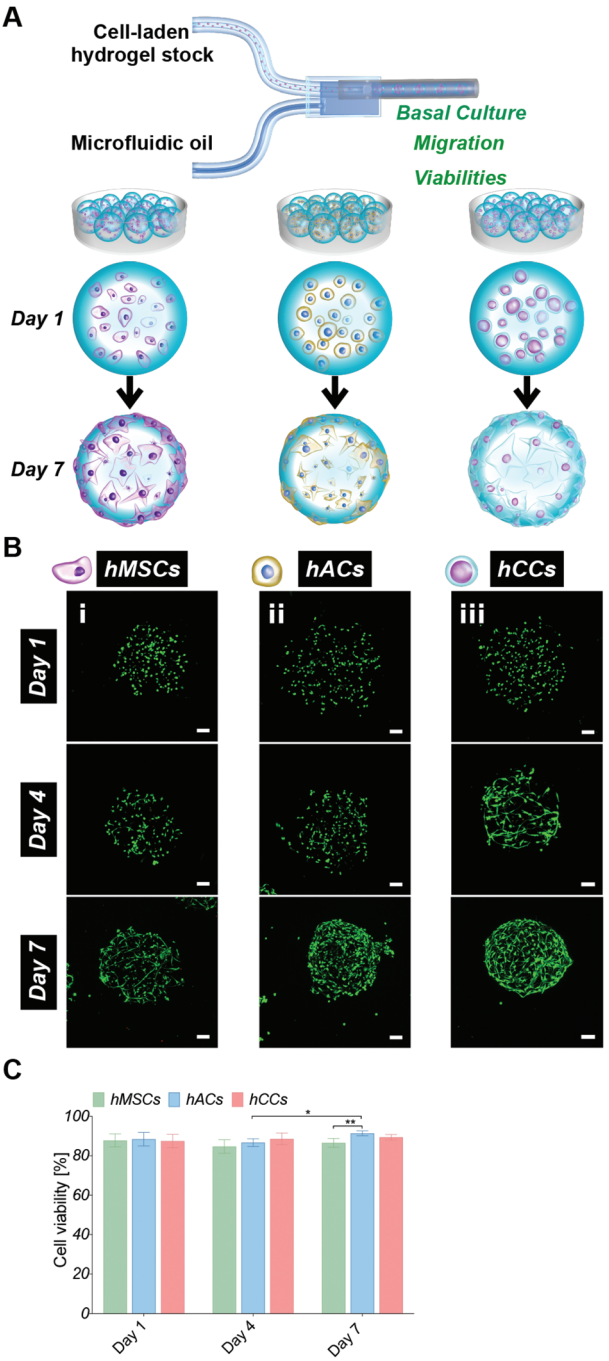

Fig. 1 (A) Schematic representation of microfluidic *in situ* microencapsulation of human cells (hMSCs, hACs and hCCs) for cell screening analysis. (B) Live/dead staining of cell-laden microgels on day 1, 4, and 7 (i: hMSCs, ii: hACs and iii: hCCs, z-stack fluorescent images showing live cells in green and dead cells in red, scale bar: 100 μm. (C) Quantitative measurements of hMSC, hAC and hCC viabilities in microgels (*P < 0.05 and **P < 0.01).

exchange.[13,19,40,41] This highly efficient mass transfer property is therefore considered an additional benefit to enhance the biocompatibility of the microgels.

Cell migration behaviour in the microgels was monitored over 7 days by analysing the fluorescent intensity profiles of 3D

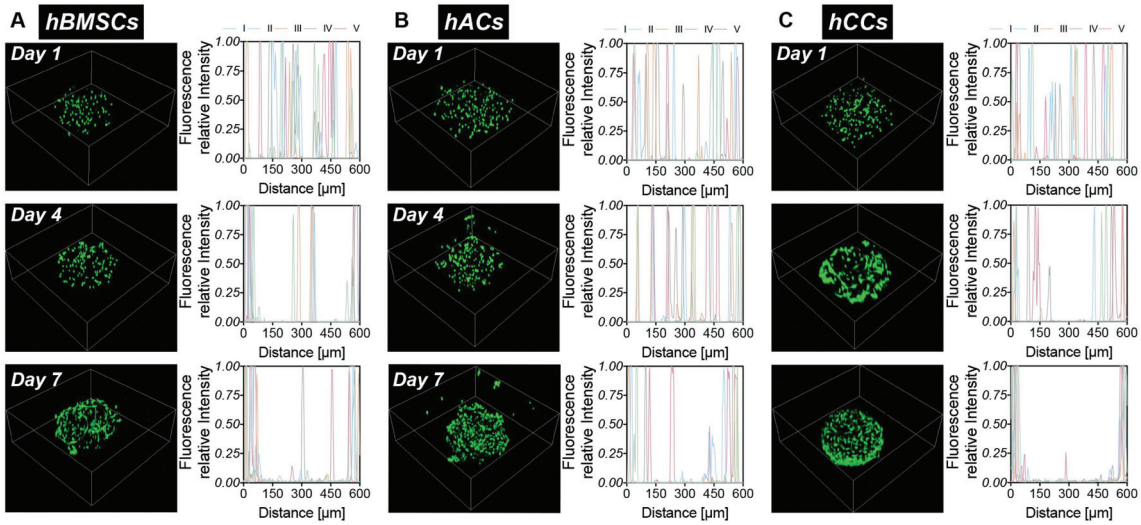

Fig. 2 hMSC, hAC and hCC migration in the microgels – 3D reconstruction images of live/dead staining and intensity profile analysis for 5 samples (I, II, III, IV and V represent different samples) of the middle slice of the microgels on day 1, 4 and 7. (A) hMSCs. (B) hACs. (C) hCCs.

reconstruction images (Fig. 2). At day 1, cells were homogenously distributed in the microgels, confirming that the droplet pipette-tip based microfluidic technique allowed uniform cell microencapsulation. Additionally, analysis of the cell morphologies indicated very few cell protrusions at day 1. This is likely due to the cells requiring more time to fully sense, adapt to and interact with the surrounding matrix. Surprisingly, after four days in culture, obvious differences in cell distribution were already observed between the three different cell types. There were several hMSCs relocated close to the microgel surface but still some cells residing near the core (Fig. 2A). However, there was no noticeable change to the hAC intensity profile compared to day 1, which indicated that the uniform distribution of hACs was maintained (Fig. 2B). Conversely, all the hCCs were found at the microgel periphery with no cells in the centre (Fig. 2C). This observation suggests that hCCs migrate faster than hMSCs and both migrate to a greater extent than hACs. Contrary to the cellular morphologies at day 1, protrusions were evident in all three cell types at day 4, suggesting that the cells had started to spread and interact with the surrounding matrix.

After one week in culture, in line with our previous findings,[22] the majority of hMSCs were located near the microgel surface with only a few at the core (Fig. 2A). Almost all hCCs had migrated to the microgel surface and the hACs had also now migrated away from the interior of the microgels with less in the core. In terms of morphology, both hCCs and hMSCs presented longer membrane protrusions than hACs. This difference in filopodial extension observed in Fig. 1Bi–iii could be due to the presence of more hCCs and hMSCs located at the surface of the microgels, leading to fewer constraints from the surrounding gel matrix and more cell–cell contacts compared to hACs within the gel. Another possible reason is the different expression levels of migratory factors such as matrix metalloproteases and integrins.[42]

Overall, the gelatin microgels provided both a cytocompatible and dynamic microenvironment, enabling long-term survival and migration of all three cell types. Here, hCCs demonstrated the most rapid migration to the microgel surface. Based on our previous findings, which show that tissue formation is driven by hMSCs that migrate into the spaces between the microgels, it was hypothesised that the high migratory behaviour of hCCs would lead to rapid cartilage tissue regeneration in the gelatin microgel system. This fast migration capacity of hCCs appears to be well supported by their original isolation process.[37] Briefly, hCCs are derived from cells which migrated out of a cultured piece of proximal ulnar epiphysis tissue explant from a 14-week gestation donor. Hence, it seems likely that the cell selection process favours a cell type that possesses a rapid migration ability. In addition to their fast migration, hCCs are considered to be an emerging cell source for cartilage regeneration which avoids donor-to-donor variations and makes them particularly attractive for clinical applications.[32,37] hCCs were consequently selected over hMSCs and hACs for the subsequent *in vitro* and *in vivo* chondrogenic studies.

2.2. hCC-laden bulk hydrogel and microgel chondrogenic differentiation *in vitro*

hCC-laden microgels were assembled by reacting microgels with 4-arm PEG-NHS ("NHSA-microgels") and the *in vitro* chondrogenic potential was assessed. The bulk hydrogels and NHSA-microgels were cultured for three weeks in chondrogenic media ((+)TGF-β1) or in (+)TGF-β1 media for the first week before being switched to chondrogenic control media ((−)TGF-β1) for the following two weeks (Fig. 3A).

2.2.1. Gene expression analysis of hCC chondrogenesis *in vitro*. RT-qPCR was performed on cells harvested at day 1, 7 and 21, to examine the expression of chondrogenic markers. After one week of chondrogenic culture, a significant upregula-

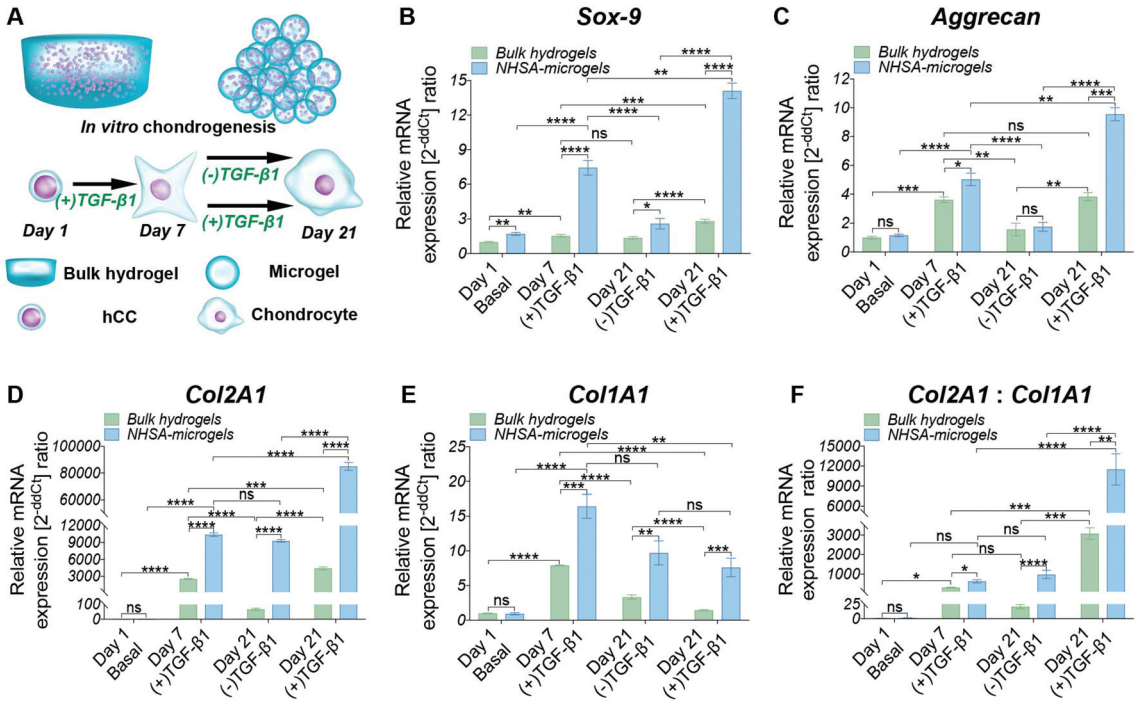

Fig. 3 (A) Schematic representation of hCC-laden bulk hydrogel and NHSA-microgel *in vitro* chondrogenesis: either cultured in chondrogenic media ((+)TGF-β1) for three weeks or in chondrogenic media ((+)TGF-β1) for the first week and control media ((–)TGF-β1) for the following two weeks. RT-qPCR analysis of hCC chondrogenesis in bulk hydrogels and NHSA-microgels was done after 1, 7 and 21 days of culture. (B–E) The fold changes of Sox-9, Aggrecan, Col2A1 and Col1A1 are expressed using RPL13a as the reference gene. (F) The chondrogenic differentiation index (gene expression ratio of Col2A1 and Col1A1). *$P < 0.05$, **$P < 0.01$, ***$P < 0.001$, and ****$P < 0.0001$.

tion of the target genes Sox-9, Aggrecan and Col2A1, normalized to the reference gene RPL13a, was observed in both bulk hydrogel and NHSA-microgels (Fig. 3B–D). The expression levels of these genes, in both bulk hydrogels and NHSA-microgels, dramatically decreased by day 21 upon culture in TGF-β1-free media (referred to as "(–)TGF-β1" media) for the final two weeks. However, it is remarkable that these reduced values were still higher than day 1 samples, suggesting that some level of chondrogenesis might continue even without continuous TGF-β1 supplementation. In contrast to (–)TGF-β1 cultured samples, a continuous increase in Sox-9, Aggrecan and Col2A1 gene expression was achieved in the samples continuously cultured in (+)TGF-β1 media.

Continuous supplementation of TGF-β1 led to a steady increase in chondrogenic gene expression in microgels and, to a lower extent, in bulk hydrogels. However, Aggrecan gene expression in hCCs encapsulated in bulk hydrogels and cultured in (+)TGF-β1 media for three weeks did not show significant increase compared to one-week culture (Fig. 3C, $P = 0.9869$). This may indicate that hCCs had reached a peak expression level of Aggrecan after one week culture in the bulk hydrogel, which could only then be maintained with prolonged TGF-β1 supplementation. Although a decrease of chondrogenic gene expression could be expected upon stopping growth factor supplementation, no significant reduction of Col2A1 expression level was observed in the NHSA-microgels after TGF-β1 withdrawal ($P = 0.6497$). This indicates that following one week preculture in (+)TGF-β1 media, hCCs are able to maintain a high level of Col2A1 expression for at least 2 weeks *in vitro* without additional TGF-β1 supplementation. This was particularly encouraging for the following *in vivo* studies that hCC preculture in NHSA-microgels in (+)TGF-β1 media would be expected to promote sustained chondrogenic differentiation.

In addition to the differences in (+)TGF-β1 *vs.* (–)TGF-β1 treatment regimes, significant differences were also identified between the bulk hydrogels and NHSA-microgels. Sox-9, Aggrecan and Col2A1 expression in NHSA-microgels were substantially higher than in the bulk hydrogels from the same media, at each time point. This demonstrates the superiority of NHSA-microgels compared to the bulk hydrogels for hCC chondrogenesis. The most striking result was the vastly increased expression of the Col2A1 gene in NHSA-microgels (Fig. 3D). Compared to day 1 samples, hCCs cultured in NHSA-microgels for 7 days exhibited more than 10 000-fold elevation of Col2A1 expression, which further increased with continuous TGF-β1 supplementation to yield an approximately 85 000-fold upregulation at day 21. This was 20 times higher than the 4000-fold upregulation in bulk hydrogels. Type-II collagen has been identified as the most predominant component in articular cartilage[43] and the exceptionally elevated expression of Col2A1 indicates promising cartilaginous matrix deposition in the NHSA-microgels. Given that this remarkable Col2A1 expression upregulation was also observed in our previous studies with hMSCs microencapsulation,[22,23] we conclude that

the effects are due to the spherical geometry, small dimensions of the microgels and therefore increased mass transport in the microgel system, rather than the source of microencapsulated cells.

In addition to the typical chondrogenic markers, Col1A1 was monitored to examine the quality of the chondrogenic differentiation (Fig. 3E). Interestingly, in both bulk hydrogel and NHSA-microgels, the highest upregulation of Col1A1 was obtained at day 7, with levels subsequently decreasing in both (+)TGF-β1 and (−)TGF-β1 media. This indicates that the hCCs might be in the early chondrogenic condensation process during the first week, a period in which cell–cell interactions are formed similarly to the process of fetal chondrogenesis, associated with type-I collagen production.[44] The decrease of Col1A1 expression from day 7 to 21 may indicate the initiation of hyaline-like cartilage tissue development, in which the ratio of type-I: type-II collagen is reduced. Col1A1 was also compared with Col2A1 to determine the chondrogenic differentiation index (Col2A1 : Col1A1) (Fig. 3F). Higher type-II collagen gene expression level was observed in all samples compared to the type-I collagen regardless of time point or geometry, which is suggestive of hyaline type cartilage formation in these systems. However, the differentiation index in the NHSA-microgels was significantly higher than bulk hydrogels (P = 0.0004), which aligns well with previous chondrogenic genes results, and further substantiates that the NHSA-microgels were better than the bulk hydrogel for hCC chondrogenesis.

Generally, the Sox-9, Aggrecan and Col2A1 gene expression levels were higher in NHSA-microgels compared to the bulk hydrogel, confirming that NHSA-microgels provide a better microenvironment for hCC chondrogenesis compared to bulk hydrogels. Even though the chondrogenic gene expression levels were attenuated without continuous supplementation of TGF-β1 in the culture media, the absolute expression value remained significantly higher than the normalised conditions, which implied that chondrogenic differentiation of hCCs was not terminated or reversed.

2.2.2. Biochemical analysis of hCC chondrogenesis *in vitro*. hCC chondrogenesis in NHSA-microgels was also characterised by quantifying the chondrogenic capacity of the cells in the gel. The production of GAGs in bulk hydrogels and NHSA-microgels were measured *via* the biochemical DMMB assay (Fig. 4). Increased chondrogenic potential was observed in both bulk hydrogels and NHSA-microgels after one week in chondrogenic culture media. GAGs were continuously deposited by hCCs and accumulated in either bulk hydrogels or NHSA-microgels even without continued TGF-β1 supplemented in the media. These results are consistent with the upregulation of chondrogenic genes in the samples cultured in (−)TGF-β1 media after one week of chondrogenic induction. In general, both bulk hydrogels and NHSA-microgels provided a favourable microenvironment for hCC culture, supporting matrix remodelling and deposition of cartilaginous matrix. In contrast to the results for chondrogenic gene expression, a higher chondrogenic potential of hCCs in the bulk hydrogel was observed compared to NHSA-microgels. Notably, the chondrogenic capacity in the bulk hydrogel increased by 500% (P < 0.0001) from basal levels after seven days in culture, but reached approximately 400% in the NHSA-microgels (P = 0.0141). Similarly, after three weeks culture in chondrogenic media, the highest chondrogenic potential was achieved in bulk hydrogels, at 10 times the amount of that in day 1 cultures. This was significantly higher than the NHSA-microgels cultured at the same condition (P = 0.0323). We believe that this discrepancy between Aggrecan gene expression and biochemical quantification of GAGs is a consequence of the highly porous structure of the assembled NHSA-microgels. It is possible that some of the deposited GAGs diffused out of the NHSA-microgels through the porous structure into the culture media, thus leading to less overall GAGs accumulation as compared to the constrained nanoporous bulk hydrogel condition. Moreover, in NHSA-microgels, the majority of cells migrated to the surface of the microgels. Thus, the matrix could only be deposited in the limited space in between the microgels with less available volume than the bulk hydrogel. A number of studies have reported that the GAG yield and cartilage function have a non-linear correlation[45,46] and so the GAG content detected in either bulk hydrogel or NHSA-microgel cannot be directly correlated with the regenerated tissue quality.

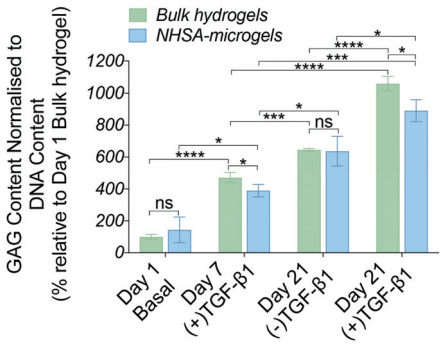

Fig. 4 Biochemical analysis in bulk hydrogels and NHSA-microgels over 21 days in *in vitro* culture. Values represent DMMB assay measurements of GAG accumulation normalised to DNA content (*P < 0.05, **P < 0.01, ***P < 0.001, and ****P < 0.0001).

2.2.3. Histological analysis of hCC chondrogenesis *in vitro*. Histological analysis was conducted to characterize the newly deposited ECM in bulk hydrogels and NHSA-microgels. Alcian blue staining was performed to assess the GAG distribution (Fig. 5A). Consistent with the calcein staining at day 1, hCCs were rounded and homogeneously distributed in both bulk hydrogels and microgels. The day 1 timepoint is too early for noticeable GAG deposition to occur and only showed the background staining (Fig. 5Ai & ii). After one week of chondrogenic culture, cells were still evenly distributed in the bulk hydrogel (Fig. 5Aiii), while in NHSA-microgels the majority of cells were located at the microgel periphery or in the cavities between the microgels. These cells showed extensive spreading (Fig. 5Aiv), which is consistent with previous viability and migration data (Fig. 1). With the NHS-crosslinking, the microgel bonding between the gels was apparent, with the existence of a highly

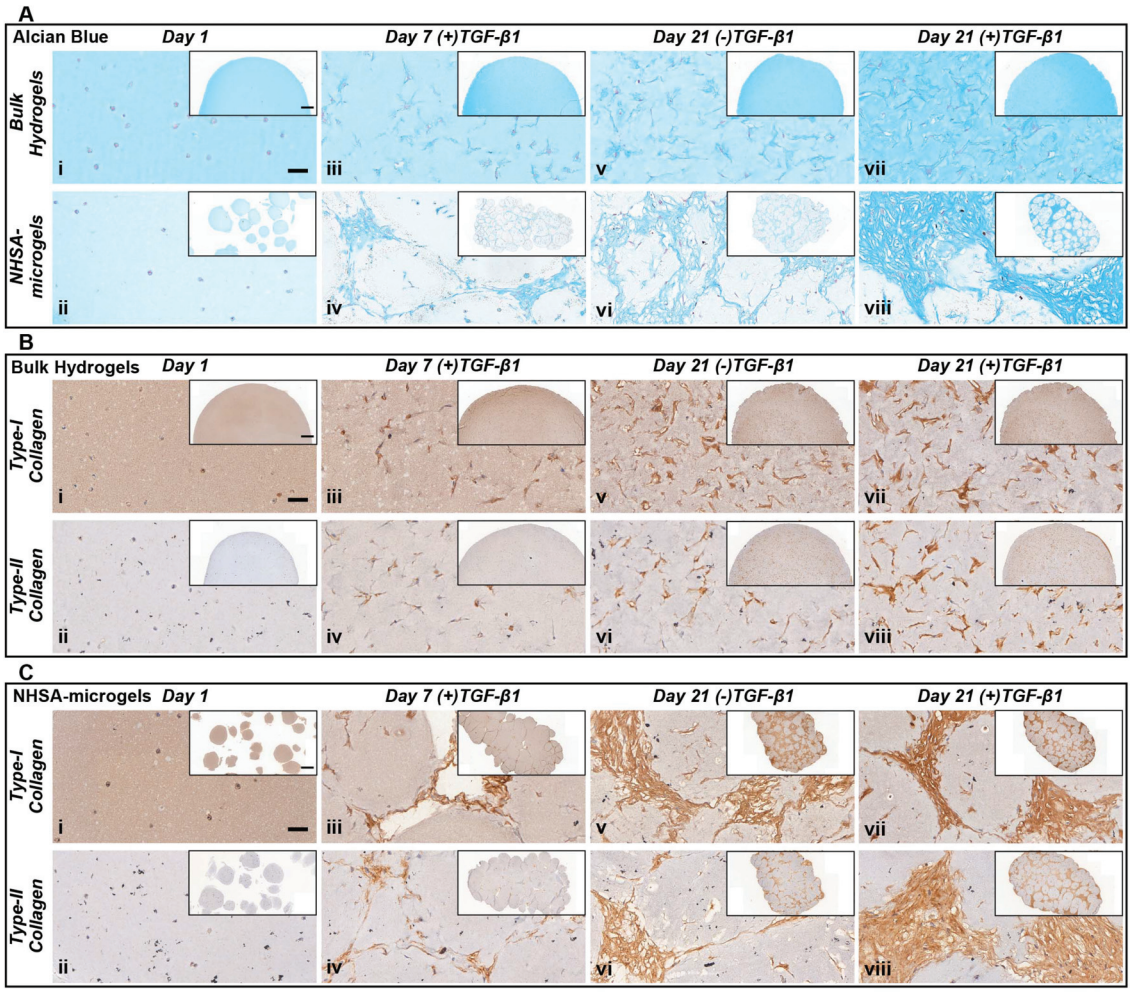

Fig. 5 Histological characterisation of bulk hydrogels and NHSA-microgels at day 1, 7 & 21 of *in vitro* culture. (A) Alcian blue (pH 1) staining – bulk hydrogel (top row) & NHSA-microgels (bottom row). (B) Type-I and type-II collagen immunohistochemical staining on bulk hydrogels. (C) Type-I and type-II collagen immunohistochemical staining on NHSA-microgels (scale bar: 50 μm/inset: 500 μm).

porous structure. Although the samples were only cultured for one week, positive staining for GAGs could already be observed in both bulk hydrogels and NHSA-microgels and showed a pericellular distribution. After two additional weeks in culture, all samples showed more intense Alcian blue staining, suggesting further deposition of cartilaginous matrix. In bulk hydrogels, cells cultured in the (−)TGF-β1 media were more spread at day 21 than at day 7 and GAGs were still predominantly located in the pericellular area (Fig. 5Av). Samples cultured in (+)TGF-β1 media (Fig. 5Avii) exhibited a more intense blue staining throughout the whole gel, as compared to samples cultured in (−)TGF-β1 media. This suggests that the continuous supplementation of TGF-β1 is necessary to maintain high levels of cartilage tissue deposition. This correlated with the DMMB results that showed more GAGs production in samples cultured with continuous TGF-β1 supplementation, as compared to samples cultured in TGF-β1 free media after one week of chondrogenic induction.

In NHSA-microgels, the most intense Alcian blue staining was located in the cavities between the microgels (Fig. 5Avi & viii), showing that most GAGs were deposited in these spaces rather than within the hydrogel matrix. This was expected since the cells had already migrated out of the gelatin microgels and proliferated in the macropores, as evidenced by the few nuclei (nuclear fast red staining) inside the microgels. Similar to bulk gels, the most intense staining was observed in the (+)TGF-β1 media-cultured samples as compared to those without continuous TGF-β1 supplementation (Fig. 5Aviii). The (+)TGF-β1 media-cultured samples formed a highly condensed tissue structure, particularly in the gaps between the microgels, while the gaps in between the (−)TGF-β1 media-cultured microgels were filled with relatively loose matrix. This further supports the observation that hCCs require continuous exposure to TGF-β1 to more effectively undergo chondrogenesis. Nevertheless, in both (+)TGF-β1 and (−)TGF-β1 media, NHSA-microgels displayed a lack of positive staining close to the hCC pericellular region, which demonstrated a pocket morphology formation within the newly formed matrix. This feature is similar to the mature chondrocytes living in lacunae within a typical articular cartilage tissue.[47] Although hCCs on

the surface of microgels were highly stretched and in close contacted with each other, the cells in the newly formed tissue between the microgels adopted a more rounded morphology and were sparsely distributed. Due to the close resemblance of this structure to native articular cartilage, these phenotypes were believed to be the additional evidence for hyaline type cartilage formation in the NHSA-microgels, upon further remodelling and gelatin microgel resorption.[48]

Type-I and type-II collagen levels and distribution were also monitored throughout the culture period (Fig. 5B & C). After one week of culture, there was positive staining for both type-I and type-II collagen in all samples, with a distribution at the intracellular and pericellular territories. In the bulk hydrogel, type-II collagen remained located at the pericellular environment at day 21 in either (+)TGF-β1 or (−)TGF-β1 media. This does not follow the same trend as for the GAGs that were distributed throughout the whole bulk hydrogel (Fig. 5Bvi & viii). The morphology and distribution of type-II collagen in NHSA-microgels at day 21 was similar to the GAG deposition as defined by Alcian blue staining (Fig. 5A & C). Generally, type-II collagen was deposited in the cavities between the microgels. Samples cultured in (+)TGF-β1 media exhibited a more condensed collagen matrix structure compared to (−)TGF-β1 media. This result further confirmed that continuous supplementation of TGF-β1 stimulates hCCs to produce more cartilaginous matrix in the construct. Interestingly, the distribution and morphology of type-I collagen were identical to type-II collagen in both bulk hydrogels and NHSA-microgels. This is in contrast to our previous hMSC studies, in which significantly more type-II collagen was synthesised compared to type-I collagen.[23] Strong type-I collagen staining has also been reported in several other studies using hCCs for cartilage regeneration.[32,38] Hence, the unexpectedly high type-I collagen production may be specific to the hCC phenotype. Although the reasons for this result are not yet completely understood, one possible explanation is that the hCCs may still be in an early chondrogenic developmental stage, similar to fetal cartilage tissue which shows an extensive amount of type-I collagen.[49,50] Furthermore, Sox-9 has been recognised as an important cartilage marker to regulate early chondrogenic development. The gene expression results demonstrated sustained Sox-9 upregulation over three weeks of culture, which further supports our hypothesis that hCCs might still be undergoing early chondrogenesis in both bulk hydrogel and NHSA-microgels. Prolonged culture with further analysis of Sox9/Scleraxis expression ratio and type-I/II collagen staining,[51] may allow this hypothesis to be examined in the future and determine whether the newly-formed ECM would turn into a more like hyaline- or fibro-cartilage in terms of collagen distribution.

Taken together, the histological analyses demonstrated *in vitro* cartilaginous matrix formation in both bulk hydrogel and NHSA-microgels. Although bulk hydrogels had a higher overall GAG content, histological analysis suggests a better quality of the newly deposited ECM in the interstitial spaces within the assembled NHSA-microgels. In fact, it exhibited a structure similar to native articular cartilage tissue, in which hCCs showed a rounded morphology and were sparsely distributed, also residing in lacunae within the structure. Additionally, even though continuous supplementation of TGF-β1 to the hCCs lead to a more condensed matrix deposition, one week of pre-chondrogenic induction could already initiate chondrogenesis with continuous cartilaginous matrix production over time.

2.2.4. Biomechanical analysis of hCC chondrogenesis *in vitro*. Complementary to the analysis of tissue composition, biomechanical properties have been considered as an essential parameter to evaluate the quality of the generated cartilage tissue. Therefore, the mechanical properties of hCC-laden bulk hydrogels and NHSA-microgels were assessed *via* a nanoindentation test (Fig. 6). At day 1, the elastic modulus of the bulk hydrogel was 7.6 ± 0.3 kPa, which was significantly higher than the NHSA-microgels at 5.9 ± 0.5 kPa (P = 0.0210). The relatively weaker mechanical properties of NHSA-microgels at day 1 may be due to the presence of the highly porous structures within the assembled microgels meaning that the initial stability of NHSA-microgels is less than the bulk hydrogels.

The cell-laden bulk hydrogel cultured in the (−)TGF-β1 media for three weeks maintained an elastic modulus of 6.5 ± 0.5 kPa with no significant change compared to day 1. On the contrary, the modulus of the cell-laden NHSA-microgels cultured in (−)TGF-β1 media from day 7 to 21 was higher at the three week timepoint, reaching an elastic modulus of 9.5 ± 0.3 kPa, which was significantly higher than that of the bulk hydrogel (P = 0.0088). This indicated that the cartilaginous matrix in NHSA-microgels after three weeks culture (one week (+)TGF-β1 media and two weeks (−)TGF-β1 media) was not only histologically better, with a hyaline-like cartilaginous matrix phenotype (rounded cell morphology within lacunae, cells sparsely distributed in the dense ECM, Fig. 5A and C), but also led to a higher modulus of the NHSA-microgels samples compared to bulk hydrogels. Moreover, an increase in elastic modulus was detected in the samples that were continuously cultured in the (+)TGF-β media for 3 weeks, achieving a modulus of 16.2 ± 0.7 kPa for the bulk hydrogel and 18.8 kPa ± 1.2 kPa for the NHSA-microgels. This again suggested

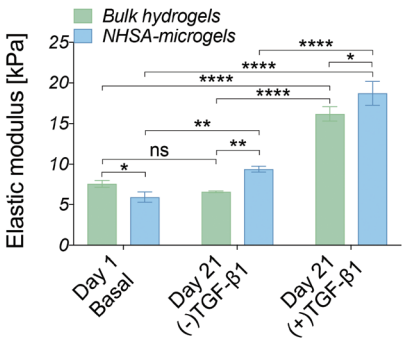

Fig. 6 Biomechanical characterisation of bulk hydrogels and NHSA-microgels using nanoindentation at day 1 & 21 of *in vitro* culture (*P < 0.05, **P < 0.01, ***P < 0.001, and ****P < 0.0001).

that continuous supplementation of TGF-β1 considerably improves chondrogenic outcomes when relying on hCCs for ECM synthesis. Taken as a whole, general maintenance or enhancement of elastic modulus was achieved in all samples after three weeks culture. Promisingly, although NHSA-microgels demonstrated a lower modulus compared to bulk hydrogels at day 1, they reached a slightly, but significantly (P = 0.0181) higher elastic modulus compared to bulk hydrogels after three weeks chondrogenesis.

Overall, based on *in vitro* gene expression, biochemical, histological and biomechanical analysis, chondrogenic differentiation of hCCs was achieved within all different samples, but showing the best results for NHSA-microgels cultured in the presence of TGF-β1 for 3 weeks.

2.3 hCC-laden bulk hydrogel and microgel implantation *in vivo*

The *in vitro* studies demonstrated the ability to initiate and maintain hCC chondrogenesis in both bulk hydrogels and NHSA-microgels by pre-culture in chondrogenic media. Therefore, in order to evaluate the scaffold stability and whether this preculture strategy could be effective in a clinical scenario, the pre-cultured samples (Fig. 7A, two weeks in (+) TGF-β1 media) were implanted subcutaneously in a nude

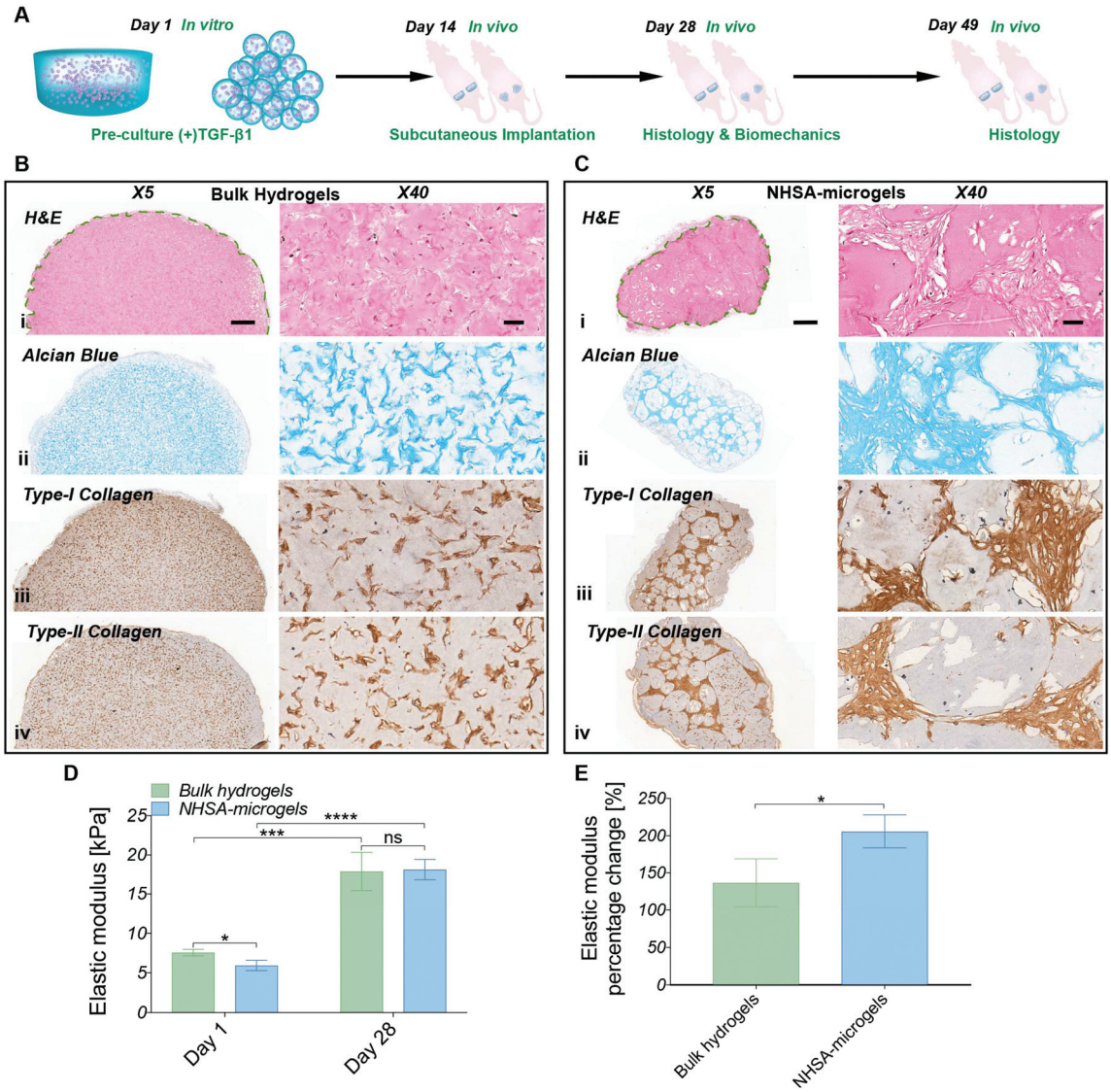

Fig. 7 (A) Schematic representation of hCC-laden bulk hydrogels and NHSA-microgel *in vivo* chondrogenesis: after *in vitro* pre-culture in chondrogenic media ((+)TGF-β1) for two weeks, samples were subcutaneously implanted into nude mice (left mice – bulk hydrogel; right mice – NHSA-microgels) and maintained *in vivo* for an additional two weeks (day 28) or five weeks (day 49). (B) Histological analysis of bulk hydrogel at day 28 (i: H&E, ii: Alcian blue, iii: type-I collagen, iv: type-II collagen). (C) Histological analysis of NHSA-microgel at day 28 (i: H&E, ii: Alcian blue, iii: type-I collagen, iv: type-II collagen) (scale bar: X5/500 μm; X40/50 μm). (D) Nanoindentation tests at day 1 and day 28. (E) Percentage elastic modulus increment profile showing hCC-laden bulk hydrogel and NHSA-microgel mechanical properties enhancement after 28 days maintenance *in vivo* (*P < 0.05, **P < 0.01, ***P < 0.001, and ****P < 0.0001).

mouse model. Histological analysis was conducted two weeks and five weeks after *in vivo* implantation. Biomechanical analysis was also performed on the samples implanted for two weeks *in vivo*. Gelatin can be degraded by matrix metalloproteinases (MMPs),[52] therefore the first question was whether the hydrogels would be stable *in vivo*. Both bulk hydrogels and NHSA-microgels were visible under the skin throughout the *in vivo* maturation period. Additionally, no apparent signs of toxicity (*i.e.* irritability and necrosis) were observed near the implanted scaffold. A typical thin fibrous capsule around the scaffold was evident macroscopically and *via* histology staining and it could easily be removed for the mechanical testing after 2 weeks (Fig. 7). There was no obvious cell infiltration from the host within the bulk hydrogel or NHSA-microgels (Fig. 7Bi & Ci).

Consistent with the *in vitro* study, after two weeks *in vivo*, the hCCs were elongated and uniformly distributed in the bulk hydrogels, whilst for NHSA-microgels most of the hCCs had a round morphology and were located in the space between the NHSA-microgels (Fig. 7Bi & Ci). In addition to cell morphology and distribution, the cartilaginous matrix distribution was also consistent with *in vitro* results. Specifically, GAGs, type-I and type-II collagens were concentrated in the intracellular and pericellular environment in the bulk hydrogels, thus leading to patterned, rather than homogeneous, histological staining (Fig. 7Bii–iv). In NHSA-microgels, the newly formed tissue occupied the inter-gel spaces and had a relatively dense structure with a morphology analogous to native articular cartilage (Fig. 7Cii–iv). Therefore, the overall morphology and distribution of regenerated tissue *in vivo* were consistent with the *in vitro* studies.

Numerous cavities were present in the microgels *in vivo*, which were not observed in the bulk hydrogel or *in vitro* studies. These cavities were generally located around the surface of the microgels, and are likely due to accelerated degradation of the microgels *in vivo*. Although the exact underlying mechanism is still not entirely clear, several possible factors may be responsible. For example, the *in vivo* environment may stimulate hCCs in the NHSA-microgels to secrete more MMPs, such as MMP-2 and MMP-9 resulting in faster degradation. There may also be a high concentration of MMPs produced by endogenous cells under the skin of the mice, which more efficiently infiltrate the NHSA-microgels due to their highly porous structure. Although the accelerated *in vivo* degradation may shorten the survival time of the scaffold, this may enhance the tissue development and remodelling process to achieve a more uniform cartilaginous matrix distribution because the microgels would be eventually replaced by the regenerated ECM.

Similar to the histological analyses, the *in vivo* biomechanical analysis was consistent with previous *in vitro* studies showing that the production of the cartilaginous matrix resulted in an increase in elastic modulus of the scaffolds (Fig. 7D). After two weeks *in vitro* preculture and another two weeks *in vivo*, NHSA-microgels had an elastic modulus of 18.1 ± 1.1 kPa compared to 17.9 ± 2.0 kPa for the bulk hydrogel, which was comparable to previous *in vitro* results with a maximum of 18.8 kPa ± 1.2 kPa. Although, a similar final modulus was achieved in bulk hydrogels and NHSA-microgels, NHSA-microgels achieved a 2-fold increase in elastic modulus compared to the starting point, which was significantly higher than the change in bulk hydrogels with 1.3-fold upregulation (Fig. 7E, $P = 0.0375$).

After five weeks *in vivo*, the implanted bulk hydrogel and NHSA-microgels were still visible under the skin with no macroscopic signs of inflammation or toxicity (Fig. 8A & B). In bulk hydrogels, in contrast to the elongated shape of the cells *in vitro* and after 2 weeks *in vivo*, hCCs adopted a more rounded shape (Fig. 8Ci). In the NHSA-microgels, the individual microgels were almost fully degraded and replaced by ECM, explaining the disappearance of the overall granular structure of the samples. This resulted in a more uniform cell distribution throughout the newly formed tissue (Fig. 8Di). Of note, this remodelling of the gelatin material by the cells led to a shrinkage of the samples, which would have to be compensated by injection of more material in the defect than the volume of the lesion, in the clinical context.

Alcian blue and collagen staining demonstrated homogenous distribution of both GAGs and collagens within the entire bulk hydrogels, but none in the intracellular/pericellular regions (Fig. 8Cii–iv). This was also observed in the NHSA-microgels with cartilaginous matrix uniformly distributed across the whole construct (Fig. 8Dii–iv), which was assumed to be a result of the active cell–material interactions. This reinforced our previous observation that a more uniform cartilaginous matrix could be formed with prolonged culture. Although a native articular cartilage morphology was regenerated in NHSA-microgels, the levels of type-I collagen were still high in comparison to type-II collagen levels in both bulk hydrogels and NHSA-microgels (Fig. 8Ciii, iv & 8Diii, iv). This might be due to a lack of continuous chondrogenic induction in the *in vivo* environment, meaning that more than two weeks preculture might be necessary to fully support differentiation. More encouragingly, even though both bulk hydrogels and NHSA-microgels experienced extensive cellular remodelling and degradation, no vascularisation was evident in the NHSA-microgels after five weeks *in vivo* (Fig. 8Ci & Fig. S3†), which conforms to the characteristic of native articular cartilage tissue, in which blood vessels are absent. However, vascularisation was observed in the bulk hydrogels (Fig. 8Di & Fig. S3†). This suggested that the deposited cartilaginous matrix in NHSA-microgels was phenotypically more stable than the matrix in bulk hydrogel.

In summary, there were differences of distribution and morphology in newly formed ECM between the bulk hydrogels and NHSA-microgels after two weeks *in vivo* with NHSA-microgels being better. Although this had evened out by five weeks *in vivo*, showing similar matrix phenotype in bulk hydrogels and NHSA-microgels, the regenerated tissue in NHSA-microgels demonstrates superior quality compared to the bulk

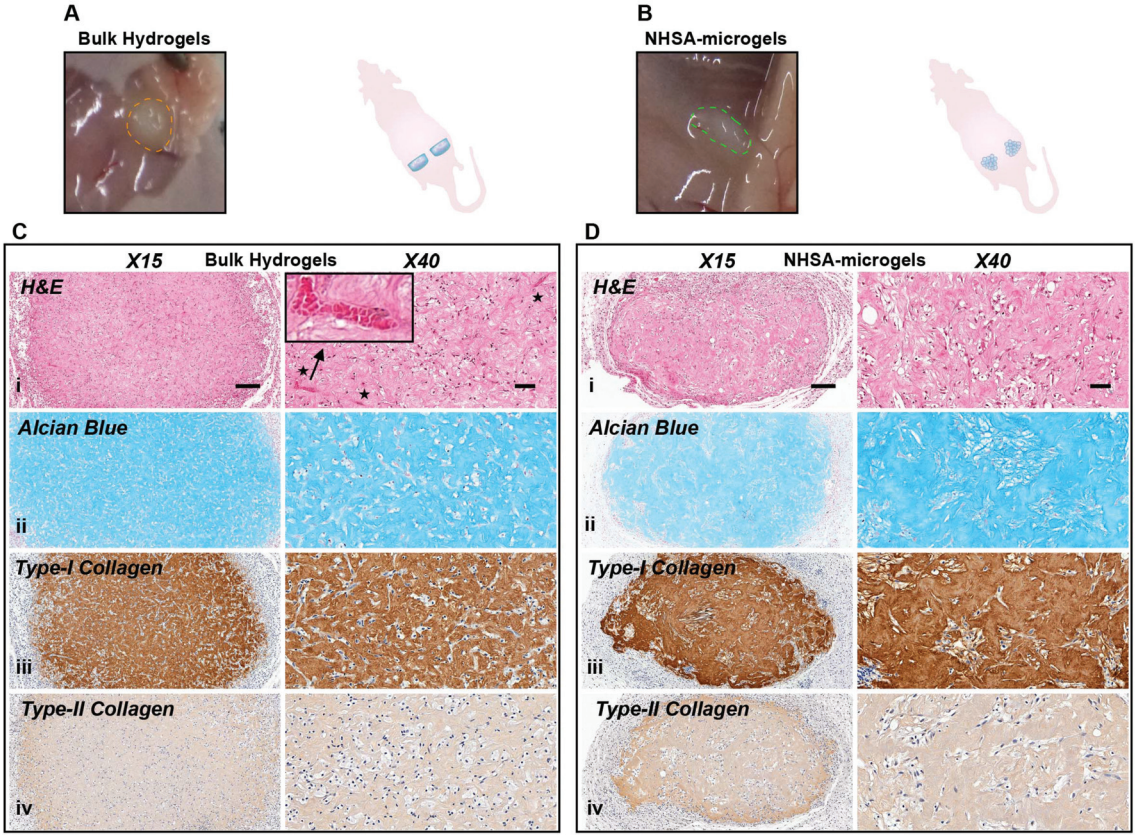

Fig. 8 hCC-laden bulk hydrogels and NHSA-microgels after *in vivo* chondrogenesis at day 49. (A and B) Appearance of bulk hydrogel & NHSA-microgel explants. (C and D) Histological analysis of bulk hydrogels & NHSA-microgels (i: H&E, ii: Alcian blue, iii: type-I collagen, iv: type-II collagen; scale bar: X5/500 μm; X40/50 μm).

hydrogel with the ability to resist vascularisation standing out.

Overall the data are encouraging and it is likely that further optimisation of pre-transplantation culture conditions will achieve a more favourable *in vivo* outcome. For instance, a more detailed investigation of the preculture times to ensure a prolonged chondrogenesis tendency and improved cartilaginous matrix retention *in vivo* is warranted. Moreover, physical entrapment or covalent conjugation of chondrogenic growth factors within the microgel network may provide an alternative approach to deliver sustained chondrogenic signals to encapsulated hCCs within the *in vivo* environment. Apart from chondrogenic supplementation, both the bulk hydrogel and NHSA-microgels experienced shrinkage after three weeks *in vitro* culture or five weeks *in vivo* maturation, which is crucial consideration for implementation into clinical practice. This is most likely due to the progressive degradation of the hydrogel materials, remodelling and formation of condensed tissue during the chondrogenesis process. In short, these preliminary *in vivo* findings follow the major outcomes in the *in vitro* studies. The encouraging preliminary *in vivo* discoveries have demonstrated the great potential of using hCC-laden NHSA-microgels for further clinical translation in articular cartilage regeneration.

3. Conclusions

In this work, the successful long-term culture of hACs, hCCs and hMSCs demonstrated the versatility of gelatin-based microgels for cell encapsulation. Based on their high viability and fast migration rate, hCCs were further investigated as an alternative emerging candidate for cartilage regeneration in combination with the microgel assembly approach. These cells were successfully microencapsulated and their ability to support chondrogenesis determined *via* the comparison to bulk hydrogels with different TGF-β1 regimes during *in vitro* culture and maintenance *in vivo*. All samples incubated either *in vitro* or *in vivo* demonstrated the ability to support cartilage formation to varying extents. *In vitro* culture experiments suggested hCCs have considerably better chondrogenic outcomes in NHSA-microgels compared to bulk hydrogels as evidenced by the significantly higher chondrogenic gene expression, a more native cartilage tissue-like structure and superior mechanical properties. Another important finding from the *in vitro* study was that the sustained supplementation of TGF-β1 during culture would greatly enhance the chondrogenesis of hCC outcomes in both bulk hydrogels and NHSA-microgels. Furthermore, there were marked differences after two weeks *in vivo* with NHSA-microgels showing better tissue

morphology and a higher degree of mechanical improvement compared to the bulk hydrogels. The newly formed tissue was more similar between bulk hydrogels and NHSA-microgels after five weeks maintenance *in vivo* but the NHSA-microgels demonstrated the ability to resist vascularisation. Overall, both *in vitro* and *in vivo* results support the utility of NHSA-microgel for hCC chondrogenesis. Therefore, it is expected that this hCC-laden NHSA-microgel system will be a promising candidate for articular cartilage repair or regeneration in the future.

4. Experimental

4.1. Hydrogel materials preparation

Gelatin was functionalised with norbornene groups with a defined substitution degree of 48% through a two-step process as described in the ESI (Fig. S1†). Norbornene carboxylic acid was first reacted with *N*-hydroxysuccinimide to produce a ester intermediate. The intermediate was subsequently grafted onto gelatin backbone to form gelatin-norbornene conjugate with further purification and lyophilised to achieve the final product. PEGdiSH crosslinker was synthesised *via* thiol functionalisation on both ends of the linear PEG with details being provided in the ESI (Fig. S2†).

4.2. Human cell types screening

4.2.1. Human adult articular chondrocytes (hACs), chondroprogenitor cells (hCCs) and mesenchymal stem cells (hMSCs) expansion. hACs were obtained from the Hirslanden Sport clinic, Zurich, Switzerland under ethics permission from the Kanton of Zurich (Ethical Approval no. KEK-ZH 2013-0097) with informed patient consent (two male- and one female-donors, aged 26–42 years). hACs were cultured in Dulbecco's modified eagle's medium (DMEM 31966) + GlutaMAXTM-I (+4.5 g L^{-1} D-glucose, +pyruvate) supplemented with 10% (v/v) FBS, 10 μg mL^{-1} gentamicin and 50 μg mL^{-1} ascorbic acid.

hCCs were isolated from a 14 weeks-gestation donor's proximal ulnar epiphysis (the same donor reported by Darwiche *et al.*,[37] Centre Hospitalier Universitaire Vaudois, Ethic Committee Protocol no. 62/07 and registered under the Federal Transplantation Programme complying with the law and Biobank procedures). Experiments in which hCCs were used were performed in accordance with the Guidelines of "Hospital Department Biobank Regulations (DAL Biobank)", and Experiments were approved by the local ethics committee (protocol #62/07: "Development of fetal cell banks for tissue engineering", August 2007). hCCs were cultured in DMEM (41966) (+4.5 g L^{-1} D-glucose, L-glutamine, +pyruvate) supplemented with 10% (v/v) FBS, 2 mM L-glutamine and 100 U mL^{-1} penicillin–streptomycin.

All MSC experiments were performed in accordance to the Guidelines of the Canton of St Gallen, Switzerland and experiments were approved by the ethics committee Kantonsspital St Gallen, Switzerland (Ethical Approval no. EKSG08/014/1B). hMSCs from 3 independent donors were isolated from femur-derived bone marrow according to the protocol in our previous report.[53] The donors were aged 42, 46, 74 years old and samples were taken during hip replacement surgery. bhMSCs were cultured in alphaMEM (+L-glutamine, – ribonucleosides, – deoxyribonucleosides) supplemented with 10% FBS, 10 μg mL^{-1} gentamicin and 1 ng mL^{-1} fibroblast growth factor 2.

All cells were expanded in a tissue culture flask and maintained at 37 °C in 5% CO_2 until passage 2 (hACs and hMSCs) or 4 (hCCs).

4.2.2. hAC, hCC and hMSC microencapsulation in microgels. All tools for microfluidic device fabrication were sterilized by UV irradiation for 1 h. The pipette tip-based microfluidic device was then fabricated in a biosafety cabinet under a sterilized environment following previously reported process[22,23] and the assembled microfluidic device was kept under sterilized conditions before use. For cell microencapsulation, hydrogel stock solutions were separately prepared as 10% (w/v) GelNB in DMEM, 15% (w/v) PEGdiSH in PBS, and 5% (w/v) lithium phenyl-2,4,6-trimethylbenzoylphosphinate (LAP, photoinitiator) in PBS. Then, corresponding amounts of hydrogel stock solutions, cell suspensions and DMEM were mixed thoroughly to achieve a 600 μL 4% (w/v) GelNB, 1% (w/v) PEGdiSH and 0.03% (w/v) LAP pre-cured hydrogel solution with the final cell density of 2.5 million cells per mL and kept warm to avoid physical gelation. The cell-laden hydrogel pre-cured mixture was loaded into a pre-warmed syringe and connected to the aqueous phase channel. Meanwhile, 3 mL of microfluidic oil (2% in FC-40, Pico-Surf™, Dolomite) was sterilized using 0.2 μm filtration, loaded into the syringe and connected to the oil phase channel. The oil phase flow rate was adjusted to 4 mL h^{-1} and pumped into the microfluidic device first to expel the air. The aqueous phase was subsequently pumped at a constant flow rate of 1 mL h^{-1} and dispersed by the oil forming the pre-cured cell-laden droplets. The harvested droplets were subsequently crosslinked *via* visible blue light irradiation (400–500 nm, 10 mW cm^{-2}) for 10 min. The photopolymerised cell-laden microgels were washed with DMEM and maintained in specific culture media according to the different cell types as previously described. Media was changed every three days.

4.2.3. hAC, hCC and hMSC viability and migration kinetics. Cell viability and migration were assessed in cell-laden microgels at day 1, 4 and 7 post-encapsulation *via* live/dead assay (Life Technologies). Briefly, culture media was removed and cell-laden microgels rinsed with warm PBS for 15 min to wash off the phenol red in the culture media. The cell-laden microgels were stained with live/dead staining solution made of 1×10^{-3} mM Calcein-AM/20×10^{-3} mM propidium iodide and incubated in the dark for 30 min at room temperature. The samples were then rinsed with PBS and imaged under a Leica SP8 confocal microscope (Inverted, Leica) taking z-stacks through a depth of 600 μm to acquire the whole microgel structure.

Fiji (https://imagej.net/Fiji) was used to create the z-stack images for the viability analysis. Viability was presented as a cell survival percentage, which was measured based on the counting of viable and dead cells. Icy software (Institut

Pasteur, Open Source, http://icy.bioimageanalysis.org/) was used to reconstruct the 3D images for the cell migration analysis. For each cell type, five microgels were selected and the intensity profiles were plotted on the middle slice of each image to assess the migration in the microgels.

4.3. Characterisation of hCCs *in vitro* chondrogenesis

4.3.1. hCCs encapsulation and chondrogenic culture. hCCs were encapsulated in both microgels and bulk hydrogels for chondrogenesis studies. hCCs microencapsulation in microgels followed the same procedures as previously described and 200 μL of microgels were cultured in a 15 mL Falcon tube (loose cap) with 2 mL culture media. For encapsulation in bulk hydrogels, the cell-laden pre-cured hydrogel solution was prepared the same way as the microgels, then 100 μL was pipetted into a home-cast PDMS cylindrical mould. The samples were subsequently exposed to visible blue light for 10 min for photo-curing. The crosslinked cell-laden bulk hydrogels were transferred into a 24-well plate and cultured with 1 mL of culture media.

Both bulk hydrogel and microgel samples were cultured in the hCC expansion media for the first 24 h. On day 1, dispersed cell-laden microgels were assembled into aggregates of microgels, referred to as "NHSA-microgels". Briefly, the culture media was first removed to reach 200 μL concentrated microgels. To this microgel suspension, 200 μL 4-arm PEG-NHS (4% (w/v)) was added and incubated for 90 min to achieve stable covalent bonding. After 1 day, NHSA-microgels and bulk hydrogels culture media was changed to chondrogenic media, which consisted of DMEM (31966) + GlutaMAXTM-I (+4.5 g L^{-1} D-glucose, +pyruvate) supplemented with 100 U mL^{-1} penicillin–streptomycin, 1% (v/v) ITS + Premix, 40 μg mL^{-1} L-proline, 50 μg mL^{-1} L-ascorbic acid-2-phosphate and 10 ng mL^{-1} TGF-β1. The samples were cultured in the chondrogenic media for seven days with media change every three days. After one week in culture, half of the samples continued to be cultured in chondrogenic media (referred as "(+)TGF-β1" media), while the other half of the samples were changed to chondrogenic control media ("(−)TGF-β1" media) with TGF-β1 withdrawn for the further two weeks.

4.3.2. Real-time quantitative polymerase chain reaction (RT-qPCR) analysis. RT-qPCR was conducted on day 1, 7 and 21 to assess the expression of chondrogenic markers by hCCs. First, bulk hydrogels and NHSA-microgels were digested by 0.5% trypsin–EDTA (Life technologies) at 37 °C for 20 min to isolate hCCs. Total RNA was extracted using a NucleoSpin® mRNA kit (Macherey-Nagel) with additional DNase treatment according to the manufacturer's instructions. The concentration and purity of the harvested RNA was analysed *via* a hybrid microplate reader (Synergy H1, BioTek Instruments), and subsequently 100 ng of RNA was reverse transcribed into 20 μL cDNA. Meanwhile, an additional reaction group without reverse transcriptase enzyme was set as no reverse transcriptase ("−RT") control.

Fast SYBR Green Master Mix (Life technologies) was used for the final PCR amplification with chondrogenesis target genes (Table S1†) and GAPDH and RPL13a were selected as housekeeping gene. Then, 10 μL SYBR, 1 μL of forward and reverse primers (150 nM each), 2 μL cDNA (5 ng μL^{-1}) and additional 7 μL DNase/RNase-free water were mixed to achieve the final 20 μL reaction mixture. All samples were prepared in triplicate and processed *via* a thermal cycler (StepOnePlus™ Real-Time PCR System). They underwent the cycling conditions of 95 °C for 20 s, 95 °C for 3 s, and 60 °C for 16 s for 40 cycles to obtain a standard melting curve. The data were analysed using the $2^{-\Delta\Delta CT}$ method normalized to day 1 bulk hydrogel samples with RPL13a as the reference gene (RPL13a was found to be more stable than GAPDH in different samples across different time points in this study, Fig. S4†).

4.3.3. DMMB and DNA analysis. The total glycosaminoglycan (GAG) content of the samples on day 1, 7 and 21 was measured by DMMB biochemistry assay. Briefly, formate buffer was first prepared by dissolving 4 g sodium formate in 4 mL formic acid and the volume was adjusted to 1 L with H_2O. Then, 80 mg of 1,9-dimethylmethylene blue (DMMB) was dissolved in 12 mL ethanol and 488 mL formate buffer to achieve the 10× DMMB stock solution. The hydrogel samples were digested in a papain solution (pH 6.5), which consisted of 1 mg mL^{-1} papain (1.5–10 U mg^{-1}, Sigma), 100 mM sodium phosphate, 5 mM EDTA and 5 mM L-cysteine at 60 °C overnight. Then, 40 μL of papain-digested lysate and 10 μL of 1% BSA/PBS were mixed and transferred into a 96-well plate with 50 μL DMMB solution (final: 2×) added. Triplicate samples were prepared for each condition and the absorbance at 525 nm was measured *via* a microplate reader (Synergy H1, BioTek Instruments) with the chondroitin 4-sulphate sodium salt (C4S from bovine trachea, Fluka) as the reference. The final GAGs contents were normalised to DNA contents. The DNA contents were determined *via* PicoGreen assay (ThermoFisher Scientific) following the manufacturer's instructions. Briefly, 40 μL of lysate was diluted in 10 μL of TE buffer (1×) and transferred into a 96-well plate with 50 μL of PicoGreen working solution added. The samples were analysed using the microplate reader (Synergy H1, BioTek Instruments) under the fluorescence mode calibrated with fluorescein wavelengths (excitation – 485 nm, emission – 525 nm) and a gradient of lambda DNA concentrations were prepared as the reference.

4.3.4. Histological analysis. Histological analysis was performed on day 1, 7 and 21 bulk hydrogels and NHSA-microgels. The samples were rinsed with PBS and fixed in 4% PFA for 30 min at room temperature. Samples were loaded into the histology cassettes and dehydrated through gradient ethanol baths (20%, 40%, 60% and 70%). The sample cassettes were loaded in an automated tissue processor (Milestone Logos J) for further dehydration and subsequently embedded in paraffin. 5 μm-thick sections of the samples were cut with a microtome (HM325, Microm). The sections were deparaffinized in xylene baths and rehydrated to water through a series of ethanol baths with decreasing concentration before histological staining.

Alcian blue (pH 1) staining was performed on the rehydrated sections following standard procedure. Briefly, slides

were acidified for 3 min in 3% (v/v) acetic acid in deionized water, then incubated for 30 min in 1% (v/v) Alcian blue in 3% (v/v) acetic acid brought to pH 1 (Sigma-Aldrich, B8438). After rinsing in tap water and counterstaining with nuclear fast red (Sigma-Aldrich N3020) for 5 min, the slides were rinsed in tap water, dehydrated and mounted with Eukritt mounting media.

Type-I and type-II collagen colorimetric staining started with antigen retrieval by digesting the section with 1200 U ml^{-1} hyaluronidase (Sigma-Aldrich, H3506) 30 min at 37 °C, followed by blocking with 5% (v/v) NGS (normal goat serum) in PBS at room temperature for 1 h. The sections were then incubated with rabbit anti collagen I (Abcam, ab138492, 1 : 1500 dilution) and rabbit anti-collagen II (Rockland, 600-401-104, 1 : 200 dilution) at 4 °C overnight. Primary antibodies were diluted in 1% (v/v) NGS in PBS. After 2 washings in PBS, slides were treated with 1% (v/v) H_2O_2 in deionized water for 20 min and goat anti-rabbit IgG-HPR (Abcam, ab6721, 1 : 1500 dilution in 1% NGS) was applied to the slides for 1 h at room temperature. After rinsing 3 times with PBS, a chromogen solution was added to the slides at room temperature using the DAB substrate kit (Abcam, ab64238), for 4 min (type-I and type-II collagens). The slides were counterstained with hematoxylin (Sigma-Aldrich, MHS1) for 3 min, washed, dehydrated and mounted with Eukritt mounting media (Sigma-Aldrich, 03989). The images of histological slides were acquired *via* a slide scanner (Pannoramic 250, 3D Histech).

4.3.5. Biomechanical analysis. To determine the biomechanical properties of the samples after chondrogenic culture, nanoindentation experiments were conducted on day 1 and 21 samples with a Bioindenter ($UNHT^3$ Bio, Anton Paar). A ruby spherical indenter (Diameter: 1 mm) was used. For each condition, triplicate samples were measured and 3 different areas were measured on each sample. The samples were completely immersed in 0.9% NaCl for testing. The maximum indentation load of 200 μN was applied to each sample with 10 s loading, 10 s holding, and 10 s unloading. The elastic moduli were calculated *via* the Bioindenter software using Hertz's model.

4.4. Characterisation of hCCs *in vivo* chondrogenesis

4.4.1. hCC-laden bulk hydrogels and NHSA-microgels subcutaneous implantation in nude mice. Cell-laden scaffolds were prepared as described above for the *in vitro* study. hCCs were encapsulated in bulk hydrogels and NHSA-microgels at a seeding density of 2.5 million cells per mL, which were precultured in (+)TGF-β1 media for two weeks before surgery. The scaffolds (2 scaffolds per animal, 6 scaffolds per condition) were subcutaneously implanted in the back of NU/NU nude female mice (from Charles River) of 3 months age. All animal studies were in compliance with the ethical guidelines of the Health Department of the Veterinary Office of the Canton of Zurich (Veterinäramt – Kanton Zurich, Switzerland, License no. ZH118/2017). Briefly, mice were anaesthetised with 4.5% isoflurane and subcutaneously injected with Meloxicam (2 mg kg^{-1}). Continuous anaesthesia (3% isoflurane) was achieved *via* a nose mask and eye cream was applied to avoid cornea damage. After 2 and 5 weeks *in vivo*, the mice were euthanised through CO_2 asphyxiation. All animal procedures were performed in accordance with the Animal Protection Ordinance of Switzerland and approved by the Veterinary Office of the Canton of Zurich (license number ZH118/2017).

4.4.2. Characterisation of hCC *in vivo* chondrogenesis. The *in vivo* chondrogenesis was characterised *via* histological and biomechanical analyses. The explants were either fixed in 4% PFA for further histology characterization (Alcian blue, type-I & -II collagen staining) or biomechanical analysis (Nanoindentation test) directly carried out as previously described.

4.5. Statistical analysis

Statistical analysis was performed using Prism 7 software. The cell viabilities were presented as mean ± standard deviation and two-way ANOVA with Tukey's *post hoc* test (equal variance) was used to determine the differences between cell types and time points. The *in vitro* qPCR and biomechanical data were shown as mean ± standard deviation with two-way ANOVA using Tukey's multiple comparison *post hoc* test. The *in vivo* nanoindentation results were demonstrated as mean ± standard deviation with unpaired t test with Welch's corrections. The data differences were considered significant when $p < 0.05$.

Conflicts of interest

There are no conflicts to declare.

Acknowledgements

F. L. acknowledges support from the New Horizons Monash-CSIRO Council [Joint PhD scholarship] and Faculty of Engineering at Monash University [Graduate research international travel grant]. M. Z. W. acknowledges the support of the Swiss National Science Foundation (315230_159783). The authors thank PD Dr med. Matthias Steinwachs for providing the healthy adult cartilage samples. We acknowledge Dr Emma Cavalli (ETH, Zurich) for isolating the hACs and expert surgical assistance. We also thank Philipp Fisch (ETH, Zurich) for sharing his knowledge on nanoindentation tests. The authors acknowledge the facilities and scientific and technical assistance of Scientific Centre for Optical and Electron Microscopy (ScopeM), ETH Zürich.

References

1 M. Krill, N. Early, J. S. Everhart and D. C. Flanigan, *JBJS Rev.*, 2018, **6**, e5.
2 Z. Ximu, Z. Wei and Y. Maobin, *Curr. Stem Cell Res. Ther.*, 2018, **13**, 497–516.
3 J. Yang, Y. S. Zhang, K. Yue and A. Khademhosseini, *Acta Biomater.*, 2017, **57**, 1–25.
4 M. Liu, X. Zeng, C. Ma, H. Yi, Z. Ali, X. Mou, S. Li, Y. Deng and N. He, *Bone Res.*, 2017, **5**, 17014.

5 K. M. C. Tsang, N. Annabi, F. Ercole, K. Zhou, D. J. Karst, F. Li, J. M. Haynes, R. A. Evans, H. Thissen, A. Khademhosseini and J. S. Forsythe, *Adv. Funct. Mater.*, 2015, **25**, 977–986.
6 N. Annabi, J. W. Nichol, X. Zhong, C. Ji, S. Koshy, A. Khademhosseini and F. Dehghani, *Tissue Eng., Part B*, 2010, **16**, 371–383.
7 L. Abune, N. Zhao, J. Lai, B. Peterson, S. Szczesny and Y. Wang, *ACS Biomater. Sci. Eng.*, 2019, **5**, 2382–2390.
8 K. J. De France, F. Xu and T. Hoare, *Adv. Healthcare Mater.*, 2018, **7**, 1700927.
9 I. K. Ko, S. J. Lee, A. Atala and J. J. Yoo, *Exp. Mol. Med.*, 2013, **45**, e57.
10 D. R. Griffin, W. M. Weaver, P. O. Scumpia, D. Di Carlo and T. Segura, *Nat. Mater.*, 2015, **14**, 737.
11 Y. Du, E. Lo, S. Ali and A. Khademhosseini, *Proc. Natl. Acad. Sci. U. S. A.*, 2008, **105**, 9522–9527.
12 E. Jain, K. M. Scott, S. P. Zustiak and S. A. Sell, *Macromol. Mater. Eng.*, 2015, **300**, 823–835.
13 X. Zhao, S. Liu, L. Yildirimer, H. Zhao, R. Ding, H. Wang, W. Cui and D. Weitz, *Adv. Funct. Mater.*, 2016, **26**, 2809–2819.
14 A. S. Caldwell, G. T. Campbell, K. M. T. Shekiro and K. S. Anseth, *Adv. Healthcare Mater.*, 2017, **6**, 1700254.
15 A. Khademhosseini and R. Langer, *Biomaterials*, 2007, **28**, 5087–5092.
16 R. M. Staruch, G. E. Glass, R. Rickard, S. P. Hettiaratchy and P. E. Butler, *Tissue Eng., Part B*, 2017, **23**, 183–198.
17 D. Sivakumaran, D. Maitland and T. Hoare, *Biomacromolecules*, 2011, **12**, 4112–4120.
18 K. Wang, S. Lin, K. Nune and R. Misra, *J. Biomater. Sci., Polym. Ed.*, 2016, **27**, 441–453.
19 C. Yu, J. Liu, G. Lu, Y. Xie, Y. Sun, Q. Wang, J. Liang, Y. Fan and X. Zhang, *J. Mater. Chem. B*, 2018, **6**, 5164–5173.
20 L. D. Solorio, E. L. Vieregge, C. D. Dhami and E. Alsberg, *Tissue Eng., Part B*, 2012, **19**, 209–220.
21 C. Luo, J. Zhao, M. Tu, R. Zeng and J. Rong, *Mater. Sci. Eng., C*, 2014, **36**, 301–308.
22 F. Li, V. X. Truong, H. Thissen, J. E. Frith and J. S. Forsythe, *ACS Appl. Mater. Interfaces*, 2017, **9**, 8589–8601.
23 F. Li, V. X. Truong, P. Fisch, C. Levinson, V. Glattauer, M. Zenobi-Wong, H. Thissen, J. S. Forsythe and J. E. Frith, *Acta Biomater.*, 2018, **77**, 48–62.
24 L. Riley, L. Schirmer and T. Segura, *Curr. Opin. Biotechnol.*, 2019, **60**, 1–8.
25 J. E. Mealy, J. J. Chung, H.-H. Jeong, D. Issadore, D. Lee, P. Atluri and J. A. Burdick, *Adv. Mater.*, 2018, **30**, 1705912.
26 E. Sideris, D. R. Griffin, Y. Ding, S. Li, W. M. Weaver, D. Di Carlo, T. Hsiai and T. Segura, *ACS Biomater. Sci. Eng.*, 2016, **2**, 2034–2041.
27 A. Sheikhi, J. de Rutte, R. Haghniaz, O. Akouissi, A. Sohrabi, D. Di Carlo and A. Khademhosseini, *Biomaterials*, 2019, **192**, 560–568.
28 S. Xin, O. M. Wyman and D. L. Alge, *Adv. Healthcare Mater.*, 2018, **7**, 1800160.
29 B. J. Huang, J. C. Hu and K. A. Athanasiou, *Biomaterials*, 2016, **98**, 1–22.
30 A. Barbero, S. Grogan, D. Schäfer, M. Heberer, P. Mainil-Varlet and I. Martin, *Osteoarthr. Cartil.*, 2004, **12**, 476–484.
31 M. Schnabel, S. Marlovits, G. Eckhoff, I. Fichtel, L. Gotzen, V. Vécsei and J. Schlegel, *Osteoarthr. Cartil.*, 2002, **10**, 62–70.
32 D. Studer, E. Cavalli, F. A. Formica, G. A. Kuhn, G. Salzmann, M. Mumme, M. R. Steinwachs, L. A. Laurent-Applegate, K. Maniura-Weber and M. Zenobi-Wong, *J. Tissue Eng. Regener. Med.*, 2017, **11**, 3014–3026.
33 E. Cavalli, C. Levinson, M. Hertl, N. Broguiere, O. Brück, S. Mustjoki, A. Gerstenberg, D. Weber, G. Salzmann, M. Steinwachs, G. Barreto and M. Zenobi-Wong, *Sci. Rep.*, 2019, **9**, 4275.
34 V. Claire, B. Carine, M. Christophe, G. Jan, B. Jean-Marc, J. Christian, W. Pierre, G. Jerome and N. Daniele, *Curr. Stem Cell Res. Ther.*, 2009, **4**, 318–329.
35 D. Studer, C. Millan, E. Ozturk, K. Maniura-Weber and M. Zenobi-Wong, *Eur. Cells Mater.*, 2012, **24**, 118–135.
36 Y. Liu, G. Zhou and Y. Cao, *Engineering*, 2017, **3**, 28–35.
37 S. Darwiche, C. Scaletta, W. Raffoul, D. P. Pioletti and L. A. Applegate, *Cell Med.*, 2012, **4**, 23–32.
38 N. Broguiere, E. Cavalli, G. M. Salzmann, L. A. Applegate and M. Zenobi-Wong, *ACS Biomater. Sci. Eng.*, 2016, **2**, 2176–2184.
39 J. Garcia, C. Mennan, H. S. McCarthy, S. Roberts, J. B. Richardson and K. T. Wright, *Stem Cells Int.*, 2016, **2016**, 11.
40 S. Ma, M. Natoli, X. Liu, M. P. Neubauer, F. M. Watt, A. Fery and W. T. S. Huck, *J. Mater. Chem. B*, 2013, **1**, 5128–5136.
41 Y. Hou, W. Xie, K. Achazi, J. L. Cuellar-Camacho, M. F. Melzig, W. Chen and R. Haag, *Acta Biomater.*, 2018, **77**, 28–37.
42 A. C. Newby, *Cardiovasc. Res.*, 2006, **69**, 614–624.
43 A. J. Sophia Fox, A. Bedi and S. A. Rodeo, *Sports Health*, 2009, **1**, 461–468.
44 W. Dessau, H. von der Mark, K. von der Mark and S. Fischer, *J. Embryol. Exp. Morphol.*, 1980, **57**, 51–60.
45 I. E. Erickson, S. R. Kestle, K. H. Zellars, M. J. Farrell, M. Kim, J. A. Burdick and R. L. Mauck, *Acta Biomater.*, 2012, **8**, 3027–3034.
46 P. A. Levett, D. W. Hutmacher, J. Malda and T. J. Klein, *PLoS One*, 2014, **9**, e113216.
47 J. B. Richardson and A. M. Bhosale, *Br. Med. Bull.*, 2008, **87**, 77–95.
48 J. D. Hayes, R. L. Brower and K. J. John, *Clin. Podiatr. Med. Surg.*, 2001, **18**, 35–53.
49 T. Kirsch and K. von der Mark, *Bone Miner.*, 1992, **18**, 107–117.
50 Y. S. Bland and D. E. Ashhurst, *Anat. Embryol.*, 1996, **194**, 607–619.
51 C. I. Lorda-Diez, J. A. Montero, C. Martinez-Cue, J. A. Garcia-Porrero and J. M. Hurle, *J. Biol. Chem.*, 2009, **284**, 29988–29996.
52 T. Rice, J. E. Larsen, H. Li, R. K. Nuttall, P. H. Larsen, S. Casha, J. Hurlbert, D. Edwards and V. W. Yong, *Neuroimmunol. Neuroinflammation*, 2017, **4**, 243–253.
53 D. Studer, S. Lischer, W. Jochum, M. Ehrbar, M. Zenobi-Wong and K. Maniura-Weber, *Tissue Eng., Part C*, 2012, **18**, 761–771.